Appl. Magn. Reson. (2008) 33, 137–152
DOI 10.1007/s00723-008-0060-5
Printed in The Netherlands

Applied
Magnetic Resonance

EPR Study of Fe^{3+}- and Ni^{2+}-Doped Macroporous $CaSiO_3$ Ceramics

R. P. S. Chakradhar[1], **B. M. Nagabhushana**[2], **G. T. Chandrappa**[2], **J. L. Rao**[3], and **K. P. Ramesh**[4]

[1] Glass Technology Laboratory, Central Glass and Ceramic Research Institute, Kolkata, India
[2] Department of Chemistry, Central College Campus, Bangalore University, Bangalore, India
[3] Department of Physics, Sri Venkateswara University, Tirupati, India
[4] Department of Physics, Indian Institute of Science, Bangalore, India

Received 25 August 2006; revised 7 August 2007

Abstract. Thermally stable macroporous $CaSiO_3$, Fe^{3+}- and Ni^{2+}-doped (0.5 to 5 mol%) ceramics have been prepared by solution combustion process by mixing respective metal nitrates (oxidizers), fumed silica. Diformol hydrazine is used as a fuel. The combustion products were identified by their X-ray diffraction and thermal gravimetry/differential thermal analysis. Single phases of β-$CaSiO_3$ and α-$CaSiO_3$ were observed at 950 and 1200 °C, respectively. The phase transition temperatures of combustion-derived $CaSiO_3$ were found to be lower compared to those obtained via solid-state reaction method. It is interesting to note that with an increase in the calcination temperature the samples become more porous with an increase in the pore diameter from 0.2 to 8 μm. The electron paramagnetic resonance (EPR) spectrum of Fe^{3+} ions in $CaSiO_3$ exhibits a weak signal at $g = 4.20 \pm 0.1$ followed by an intense signal at $g = 2.0 \pm 0.1$. The signal at $g = 4.20$ is ascribed to isolated Fe^{3+} ions at rhombic site. The signal at $g = 2.0$ is due to Fe^{3+} coupled together with dipolar interaction. In Ni^{2+}-doped $CaSiO_3$ ceramics the EPR spectrum exhibits a symmetric absorption at $g = 2.23 \pm 0.1$. This deviation from the free electron g-value is ascribed to octahedrally coordinated Ni^{2+} ions with moderately high spin–orbit coupling. The number of spins participating in resonance and the paramagnetic susceptibilities have been evaluated from EPR data as a function of Fe^{3+} as well as Ni^{2+} content. The effect of alkali ions (Li, Na and K) on the EPR spectra of these ceramics has also been studied.

1 Introduction

Porous materials are of significant interest due to their wide applications in, e.g., catalysis, separation, lightweight structural materials and biomaterials [1–5]. Since the discovery of the ordered mesoporous silica [1], a lot of porous materials have been synthesized using surfactants as a template. However, most of these materials are unstable on the removal of the surfactant and the porous skeleton collapses easily when heated above 400 °C. Therefore, new methods of synthesis which give higher stability are desirable.

As a part of our program on porous materials [5], we describe here a simple and quick method of preparing thermally stable macroporous $CaSiO_3$, Fe^{3+}- and Ni^{2+}-doped $CaSiO_3$ ceramic powders. The main advantage of this method is the ability of maintaining the porous structure even at elevated temperatures; moreover, the pore diameter increases upon heating. High thermal stability of porous materials can combine the porous structure with traditional ceramic science and technology, leading to wide applications. The demand for $CaSiO_3$-based materials is currently expanding, in particular, with respect to metallurgy companies working for aircraft, and in the context of the problem of replacing asbestos which is hazardous to health [6, 7]. In addition to this, $CaSiO_3$ is also a mineral that has many uses in numerous branches of national economies over the world. The growing demands for $CaSiO_3$ in recent years are evidenced by the steady increase in its production worldwide [8].

The study of transition metal ions (viz., Fe^{3+} and Ni^{2+}) in macroporous $CaSiO_3$ ceramics by electron paramagnetic resonance (EPR) technique gives information on the structure of macroporous $CaSiO_3$. The variations in the composition may change the local environment of the transition metal ion incorporated in macroporous $CaSiO_3$, leading to ligand field changes which may be reflected in EPR spectra. Further, in recent years, the transition metal ion doping in these materials gained importance because of interesting spectroscopic properties exhibited by them and their suitability for various technological applications.

In the present study, the synthesized powders have been well characterized by using X-ray diffraction (XRD), thermal gravimetry (TG)/differential thermal analysis (DTA), scanning electron microscopy (SEM) and EPR techniques. We have also prepared alkali-doped $CaSiO_3$ ceramic powders. We also consider the effect of iron and nickel content and that of alkali ions on spin Hamiltonian parameters as well as the site symmetry around transition metal ions in $CaSiO_3$ ceramics.

2 Material and Methods

2.1 Calculation of Stoichiometry

The starting materials used for the preparation of $CaSiO_3$ in the present study were of AnalaR grade. Calcium nitrate $Ca(NO_3)_2 \cdot 4H_2O$ and fumed silica (SiO_2 99.9%, surface area of 200 m^2/g) were the sources of Ca and Si. The stoichiometry of the redox mixture used for combustion was calculated using the total oxidizing and reducing valencies of the ingredients which serve as numerical coefficients for the stoichiometric balance, so that the equivalence ratio (ϕ_e) is unity and the energy released by the combustion is maximum [9]. According to the concept used in propellant chemistry, the valence of C is +4, H +1; divalent metal ions, +2; trivalent metal ions, +3, and so on; and O, −2. The valence of nitrogen is considered to be zero. On the basis of these considerations, calcium nitrate has an oxidizing valence of −10 and diformyl hydrazine (DFH) a reducing valence

of +8. The total valence of SiO_2 is zero. For the preparation of $CaSiO_3$, the required mole ratio of $Ca(NO_3)_2 \cdot 4H_2O$ to SiO_2 to DFH becomes 1:1:1.25.

$CaSiO_3$ ceramic powder is prepared by dissolving calcium nitrate and DFH ($C_2H_4N_2O_2$), as a fuel for combustion synthesis, which was prepared in our laboratory by the reaction of formic acid and hydrazine hydrate as described in ref. 10: in a minimum quantity of water in a cylindrical petri dish of 300 ml capacity. To this end, fumed silica was added and dispersed well using magnetic stirrer for 30 min. The heterogeneous redox mixture was rapidly heated in a muffle furnace maintained at 500 ± 10 °C. DFH is a good fuel like other N–N bonded hydrazine derivatives, e.g., carbohydrazide (CH), tetraformal trisazine (TFTA), oxalyl dihydrazide (ODH), maleic hydrazide (MH), which are known [11] to decompose to give NH_3, N_2, CO_2 and HNCO. These gaseous products along with oxides of nitrogen formed by the thermal decomposition of metal nitrates are hypergolic (spontaneously bursting into flames) at 350–500 °C. The redox mixture when heated at 500 °C boils and thermally dehydrates forming a honeycomb-like gel, which ignites to yield voluminous $CaSiO_3$ powder.

The theoretical equation assuming complete combustion of the redox mixture used for the synthesis of $CaSiO_3$ may be written as

$$4Ca(NO_3)_2 + 4SiO_2 + 5C_2H_4O_2N_2 \rightarrow 4CaSiO_3(s) + 9N_2(g) + 10H_2O(g) + 10CO_2(g) \sim 7 \text{ mol gases/}CaSiO_3.$$

Different mol% of iron- and nickel-doped $CaSiO_3$ have been prepared by using the stoichiometric formula $(50 - x)Ca(NO_3)_2 \cdot 4H_2O + 50SiO_2 + x(A(NO_3)_2 \cdot 3H_2O)$ ($0.5 \leq x \leq 5$ mol%, A = Fe or Ni) following the procedure described above. In order to investigate the effect of the alkali size on EPR signals, we have also prepared 10 mol% of alkali-doped $CaSiO_3$ ceramics.

The phase evaluation of the synthesized powders was examined with the help of X-ray powder diffractometer (Philips PW 1050/70) using Cu Kα radiation with a Ni filter. In addition to this, TG/DTA was also performed using a Netzsch simultaneous thermal analyzer. The surface morphology, size distribution of the grains of the sample was examined on a JEOL (JSM-840A) scanning electron microscope. The EPR spectra were recorded at room temperature on a JEOL-FE-1X EPR spectrometer operating in the X-band (about 9.2 GHz) with a field modulation frequency of 100 kHz. The magnetic field was scanned from 0 to 500 mT and the microwave power used was 5 mW. A powdered glass specimen of 100 mg was taken in a quartz tube for EPR measurements.

3 Results and Discussion

3.1. XRD

The phase evaluation of the solution-combustion-derived, as-formed and calcined powders of $CaSiO_3$ was carried out by powder XRD and is shown in Fig. 1.

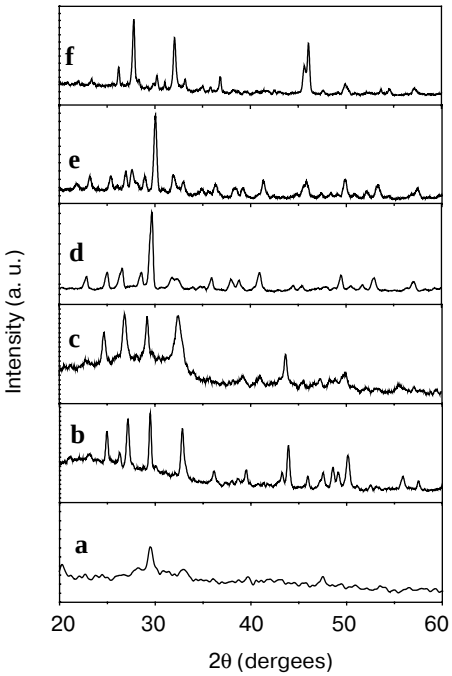

Fig. 1. Powder XRD patterns of porous $CaSiO_3$ ceramic powder: **a** as-formed, **b** 500 °C (3 h), **c** 700 °C (3 h), **d** 950 °C (3 h), **e** 1100 °C (3 h), **f** 1200 °C (3 h).

As-formed $CaSiO_3$ powder shows peaks corresponding to $CaSiO_3$ and CaO, on calcination the powders start crystallizing and give rise to a single phase β-$CaSiO_3$ (3 h at 950 °C). The peak corresponding to CaO disappears at 950 °C. Therefore, the samples calcined at 950 °C are fully crystallized and no impurity can be detected indicating a single phase of β-$CaSiO_3$. The peak positions were in agreement with literature [12, 13] and Joint Committee on Powder Diffraction Standards (27-0088). However, on further calcination (1200 °C, 3 h) a new phase is formed which may be attributed to α-$CaSiO_3$. These formation temperatures were lower than those obtained by the conventional solid-state reaction method. Yoshizawa et al. [14] reported recently in their preparation of $CaSiO_3$ by a sol–gel method that a new phase change occurred at 1200 °C while heating the gels at various temperatures and they attributed this to the conversion of β-$CaSiO_3$ to α-$CaSiO_3$.

Figure 2 shows the phase evaluation of the 1 mol% iron- and nickel-doped $CaSiO_3$ by XRD. Here also one can clearly notice that at 950 °C the iron- and nickel-doped $CaSiO_3$ exhibits the β-phase, whereas the phase transformation from β-$CaSiO_3$ to α-$CaSiO_3$ occurs at 1200 °C. The phase transition temperatures of solution-combustion-derived $CaSiO_3$ powder were found to be lower compared to the powder obtained in a solid-state reaction method [12, 15].

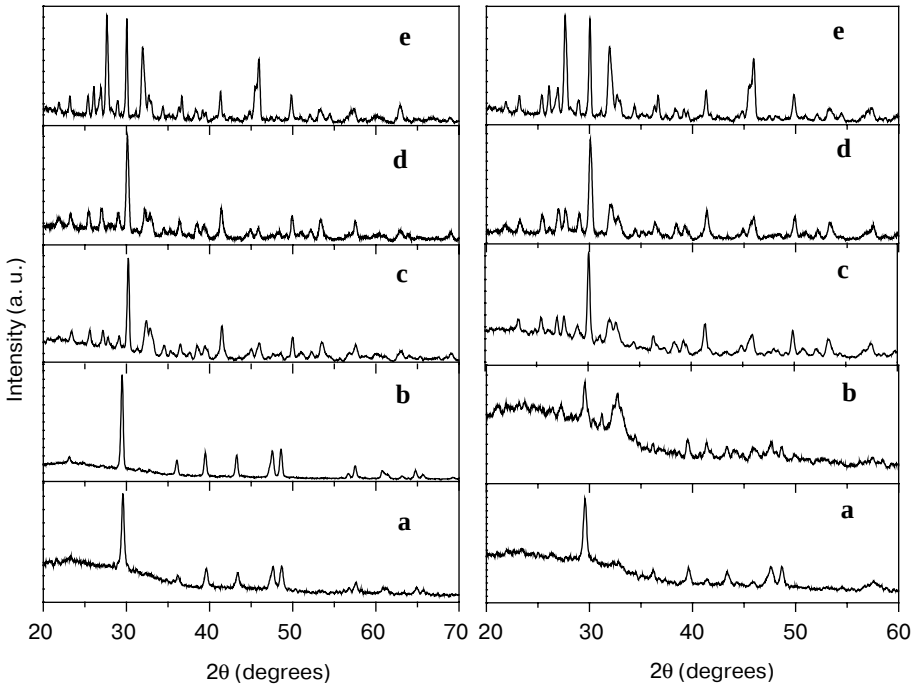

Fig. 2. Powder XRD patterns 1 mol% Fe^{3+}-doped (left) and 1 mol% Ni^{2+}-doped (right) porous $CaSiO_3$ ceramic powders: **a** as-formed, **b** 500 °C (3 h), **c** 950 °C (3 h), **d** 1100 °C (3 h), **e** 1200 °C (3 h).

In the present study, we will concentrate on β-$CaSiO_3$. Figure 3 shows the XRD patters of 1 mol% iron-doped $LiCaSiO_3$, $NaCaSiO_3$ and $KCaSiO_3$ samples calcined at 950 °C. It is interesting to observe that as the size of the alkali increases, the intensity of the XRD peaks decreases. The nominal composition of the ceramic powders was confirmed by the energy-dispersive spectroscopy technique.

The particle size of $CaSiO_3$ powders was estimated from the full width at half maximum of the diffraction peak of the powders, using Sherrer's formula [16]. It was observed that the average particle sizes of the studied samples are in the range of 29–50 nm.

3.2 DTA

DTA of as-formed $CaSiO_3$ was carried out on a Netzsch STA 409 simultaneous thermal analyzer, at the rate of 10 °C/min. The weight loss and phase changes have been studied from room temperature up to 1300 °C. The thermograms for solution-combustion-derived $CaSiO_3$ sample are shown in Fig. 4. The TG/DTA is similar to that of the $CaSiO_3$ gel reported in ref. 17. In the present study, the

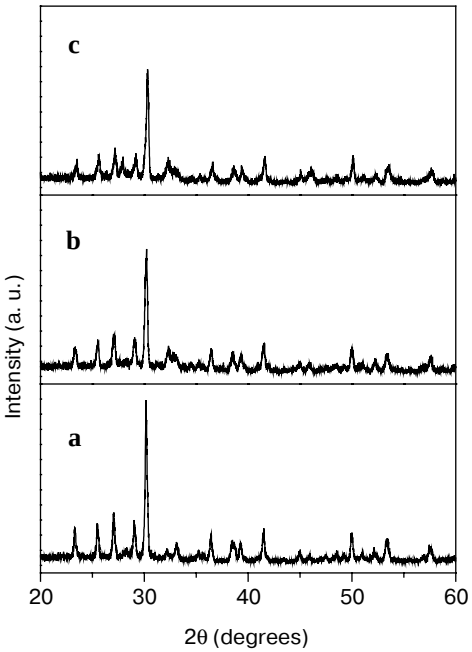

Fig. 3. Powder XRD patterns 1 mol% Fe^{3+} ions in lithium-doped $CaSiO_3$ (**a**), sodium-doped $CaSiO_3$ (**b**), potassium-doped $CaSiO_3$ sample (**c**) calcined at 950 °C.

TG curve shows about 10% weight loss at about 100 °C which can be attributed to the vaporization of adsorbed water. The exothermic peak at around 891.4 °C is attributed to starting the crystallization of $CaSiO_3$, as confirmed by XRD analysis. The second and third endothermic at about 530 °C with weight loss of about 20% and 745 °C with the weight loss of 10%, respectively, may be related to the elimination of the nitrate groups bounded to Ca and Si. The exothermic peak at 891.4 °C in the DTA curve is due to the phase transformation of β-$CaSiO_3$.

3.3 SEM

The size, morphology and distribution of the as-formed as well as calcined at 900 and 1200 °C $CaSiO_3$ powders were examined on a JEOL (S-150 Cambridge) scanning electron microscope and are shown in Fig. 5. The SEM images exhibit some interesting results. Note that with the increasing temperature (see Fig. 5) the samples become more porous and the pore diameter increases from 0.2 to 8 μm. The as-formed sample shows uniform distribution of particles; however, the samples calcined at 950 and 1200 °C exhibit particles that are a little bit agglomerated; the average agglomerated particle size of calcined $CaSiO_3$ is in the

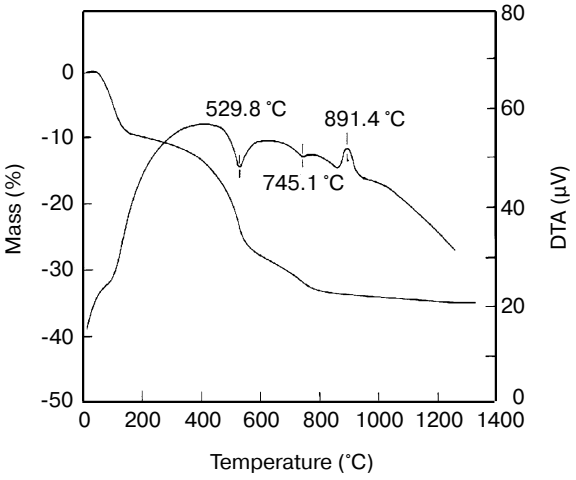

Fig. 4. TG-DTA of porous $CaSiO_3$ ceramic sample.

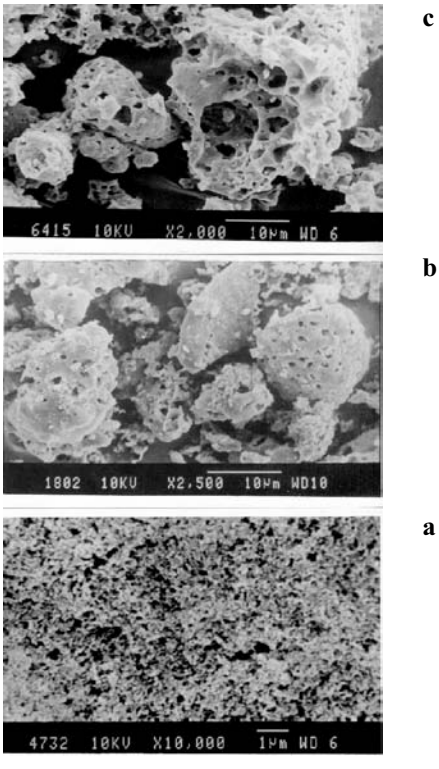

Fig. 5. SEM images of porous $CaSiO_3$ ceramic powders: **a** as-formed, **b** calcined at 950 °C for 3 h, **c** calcined at 1200 °C for 3 h.

range of 1–10 μm. With doping there is not much change in the morphology of the samples.

3.4 Porosity Measurements

The density of as-prepared and sintered $CaSiO_3$ was determined by the liquid displacement method. The percentage of porosity was calculated from the measured apparent density (D_A) according to the following equation [18]:

$$\text{Porosity} = (1 - D_A/D_T) \cdot 100,$$

where D_T is the theoretical density (2.91 g/cm^3). It is interesting to note that the porosity increases significantly with the calcination temperature, which can be seen clearly from the SEM studies. The calculated porosity values are 17.5% and 31.6% at 950 and 1200 °C, respectively. It is observed that the porosity increases significantly on calcination, which can also be seen clearly from the SEM micrographs.

3.5 Measurement of the Surface Area

The surface area is one of the important parameters used to characterize powder samples. The surface area (m^2/g) of powder samples is related with other parameters such as the particle size, shape, and surface area textures. The surface area determination involves admitting an adsorbing gas (nitrogen) to a known weight of a sample [19]. The surface area of the $CaSiO_3$ samples prepared by the combustion process was measured by a NOVA 2000 surface analyzer. The Brumauer–Emmete–Teller (BET) equation [19] describes the physical adsorption of a gas on a solid and is utilized in obtaining the surface area. The surface area of the as-formed, 950 and 1200 °C calcined samples were 31.93, 0.585 and 3.48 m^2/g, respectively. The large surface area (31.93 m^2/g) of as-formed samples is due to the uniform distribution of particles as observed in SEM micrograph. On heating the sample at 950 °C, the surface area decreases to 0.585 m^2/g which might be due to the growth in particle size or agglomeration. On further calcination at 1200 °C the surface area increases to 3.48 m^2/g, which is due to the swelling of agglomerated powder particles.

3.6 EPR Study of Fe^{3+} Ions in Porous $CaSiO_3$

No EPR signal was observed for the undoped powders, indicating that no paramagnetic impurities were present in the starting materials. When various mol% of Fe^{3+} ions were added to $CaSiO_3$ (Fig. 6), the EPR signals become observable in all investigated samples. The spectra of all investigated samples consist mainly of a weak resonance signal at $g \approx 4.20 \pm 0.10$ followed by an intense

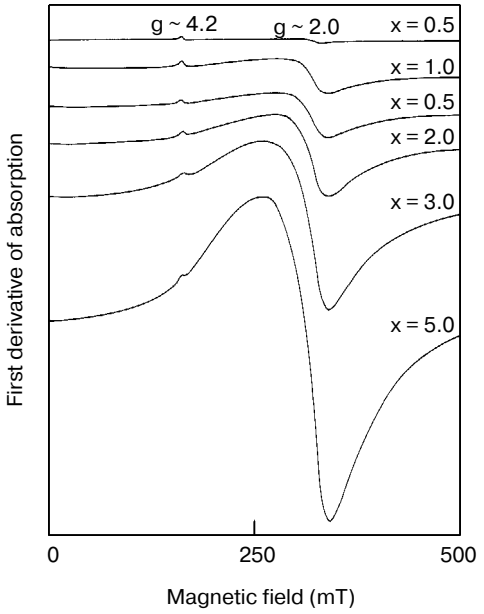

Fig. 6. EPR spectra of various mol% of Fe^{3+} ions in porous $CaSiO_3$ ceramic sample.

signal at $g = 2.0 \pm 0.1$, which is a characteristic of Fe^{3+} ions. Figure 7 shows the EPR spectra of 1 mol% of Fe^{3+} ions in lithium-doped, sodium-doped and potassium-doped $CaSiO_3$ samples. The EPR spectrum of Fe^{3+} ions in alkali-doped samples also exhibit a weak resonance signal at $g = 4.20 \pm 0.10$ and an intense signal at $g = 2.0 \pm 0.1$; further it is interesting to observe that the signal intensity is decreasing as the size of the alkali increases.

The Fe^{3+} ($3d^5$) ions in crystals have orbitally nondegenerate ^6S ground state [20–26] and exhibit zero-field splitting (ZFS) due to spin–orbit and other interactions [27–30], whereas an isotropic g value close to the free-ion value of 2.0023 is expected. However, a g-value very much greater than 2.0 often occurs; in particular, an isotropic g-value at 4.2 occurs and these large g-values arise when certain symmetry elements are present [20–23]. The theory of these large g-values is usually expressed by the spin Hamiltonian [31]

$$\mathcal{H} = \mu_B BgS + D[S_z^2 - S(S + 1)/3] + E(S_x^2 - S_y^2), \quad (1)$$

where $S = 5/2$. Here D and E are the axial and rhombic ZFS parameters.

The effective local symmetry of the ZFS Hamiltonian at the site of the Fe^{3+} ion may be characterized by the ratio $E/D = \lambda$, where λ may vary between 0 and 0.33 [29, 32–35]. $\lambda = 0$ corresponds to the axially symmetric case ($D \neq 0$, $E = 0$). An increase in λ represents a deviation from axial symmetry toward orthorhombic symmetry. Gaite and Michoulier [36] computed a relationship between g and λ that allows to obtain information on the deviation from the axial symmetry of the site from the observed resonance fields.

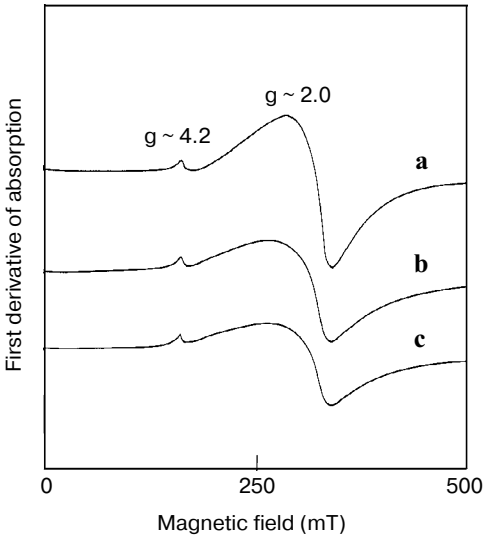

Fig. 7. EPR spectra of 1 mol% of Fe^{3+} ions in lithium-doped $CaSiO_3$ (**a**), sodium-doped $CaSiO_3$ (**b**), potassium-doped $CaSiO_3$ ceramic sample (**c**).

When Fe^{3+} impurity complexes are situated in the crystal field with a large axial component, the free-ion ^6S state splits into three Kramers doublets $|\pm 1/2\rangle$, $|\pm 3/2\rangle$ and $|\pm 5/2\rangle$ with separations usually greater than the microwave quantum. Normally, the selection rules permit EPR transitions in the $|\pm 1/2\rangle$ doublet with $g \approx 2.0$ and $g \approx 6.0$ [20, 21]. In a large number of other systems, for example, glasses and other Fe^{3+}-containing materials, a symmetric and isotropic line at $g \approx 4.0$–4.2 is observed. Castner et al. [36] explained it as arising from the middle Kramers doublet containing an admixture of different $|\pm m_j\rangle$ states, which are caused by the presence of a rhombic term $E(S_x^2 - S_y^2)$ in the Hamiltonian. According to the diagram of Gaite and Michoulier [36], λ should be close to zero to observe $g = 6.0$, i.e., the crystal field Hamiltonian and thus the ZFS one for this Fe^{3+} ion should exhibit nearly axial symmetry. In the present study we have not observed the $g = 6.0$ resonance line because of a relatively large amount of iron present in the samples. It is reported in literature that the resonance at $g = 6.0$ is observed only in samples with a very low amount of the iron content [38, 39]. The g-values observed in the present study indicate that the iron ions are in the trivalent state and the site symmetry is distorted octahedral.

In the present study, we observed a weak resonance signal at $g = 4.20 \pm 0.1$, and an intense signal at $g = 2.0 \pm 0.1$. The features of the observed EPR spectra can be qualitatively explained as follows. From the crystallographic point of view, $CaSiO_3$ belongs to the pseudo-wollastonite structure (monoclinic with the $C2/c$ space group) [40]. It is known that the wollastonite crystal structures contain single chains of tetrahedral $(SiO_4)^{4-}$ silicate. As in other single-chain silicates, two of the four oxygen anions in each tetrahedron are shared between two Si^{4+} cations to form the single chains, and the other two oxygen anions of each

tetrahedron are bonded to divalent Ca^{2+} cations. These divalent cations bond to six (or sometimes seven or eight) oxygen anions, forming octahedral coordination. In the present case, the Fe^{3+} occupies Ca^{2+} sites, which might have resulted in the distorted octahedral symmetry. It is also evident from EPR, the intense resonance peak for Fe^{3+} at $g = 2.0$ can only occur if the Fe^{3+} ions are located in a site where the crystal field interaction energy is less than the magnetic Zeeman energy. This case would correspond to iron located in a site with a higher symmetry. On the other hand, the resonance at $g = 4.2$ is due to an environment where the interaction energy between the surrounding ligands and the Fe^{3+} ion yields the ZFS energy larger than the Zeeman energy. This case would correspond to iron in a relatively low symmetry site [41–43]. Therefore, the signal at $g = 4.2$ is ascribed to isolated Fe^{3+} ions in orthorhombic site. The resonance signal at $g = 2.0$ is due to two or more Fe^{3+} ions coupled together with dipolar interaction [38, 44].

3.6.1 Calculation of Number of Spins Participating in Resonance

The number of spins participating in resonance can be calculated by comparing the area under the absorption curve with that of a standard ($CuSO_4 \cdot 5H_2O$ in this study) of known concentration. Weil et al. [23] gave the following expression which includes the experimental parameters of both sample and standard

$$N = \frac{A_x (Scan_x)^2 G_{\text{std}} (B_{\text{m}})_{\text{std}} g_{\text{std}}^2 [S(S+1)]_{\text{std}} P_{\text{std}}^{1/2}}{A_{\text{std}} (Scan_{\text{std}})^2 G_x (B_{\text{m}})_x g_x^2 [S(S+1)]_x P_x^{1/2}} [\text{Std}], \tag{2}$$

where A is the area under the absorption curve which can be obtained by double integrating the first derivative EPR absorption curve, *Scan* is the magnetic field corresponding to unit length of the chart, G is the gain, B_{m} is the modulation field width, g is the g-factor, S is the spin of the system in its ground state, P is the power of the microwave source. The subscripts x and std represent the corresponding quantities for the transition metal ions in ceramic sample and the reference ($CuSO_4 \cdot 5H_2O$), respectively.

Table 1. Number of spins (N) participating in resonance and susceptibility (χ) as a function of Fe^{3+} content in $CaSiO_3$ ceramic powders.

Fe^{3+} (mol%)	N (10^{23}/kg)	χ (10^{-2} m^3/kg)
0.5	0.12	0.3
1.0	0.13	2.4
1.5	1.28	3.1
2.0	2.38	6.2
3.0	5.51	14.6
5.0	10.36	27.5

Table 2. Number (N) of Fe^{3+} ions participating in resonance and susceptibility (χ) as a function of alkali content in $CaSiO_3$ ceramic powders.

Alkali	N (10^{23}/kg)	χ (10^{-2} m^3/kg)
Li	1.61	4.12
Na	1.57	4.05
K	1.24	3.23

Table 1 lists the variation of N with the iron content in $CaSiO_3$ ceramic powders. It is observed that N increases monotonically with iron content increasing up to $x = 5$ mol% indicating that there is no cluster formation in this system. The variation of N for 1 mol% Fe^{3+} ions in lithium-doped, sodium-doped and potassium-doped $CaSiO_3$ samples are presented in Table 2. Note that, as the alkali size is changed from Li to K, the number of spins participating in resonance decreases considerably.

3.6.2 Calculation of Paramagnetic Susceptibility from EPR Data

The EPR data can be used to calculate the paramagnetic susceptibility of the sample by the formula [45]

$$\chi = \frac{Ng^2\mu_B^2 J(J+1)}{3k_B T},$$

where N is the number of spins per cubic meter and the other symbols have their usual meaning [20–23]. N can be calculated from Eq. (2) and g is taken from EPR data. The paramagnetic susceptibilities have also been evaluated with respect to iron content as well as the alkali content and are presented in Tables 1 and 2. We chose to determine the spin susceptibility from EPR because this technique has several advantages over a static measurement, where a diamagnetic contribution must be subtracted.

3.7 EPR Study of Ni^{2+} Ions in Porous $CaSiO_3$

The EPR spectrum of Ni^{2+} ions in $CaSiO_3$ ceramics exhibits a symmetric absorption at $g = 2.23 \pm 0.01$. Figure 8 shows the EPR spectra of various mol% Ni^{2+} ions in $CaSiO_3$ ceramic powders. Figure 9 shows the EPR spectra of 1 mol% of Ni^{2+} ions in lithium-doped, sodium-doped and potassium-doped $CaSiO_3$ samples. The spectrum can be understood in the following way. The Ni^{2+} ($3d^8$) has the $^3A_2(F)$ ground state in octahedral symmetry [20–23] and the degenerate ^3F ground state splits as a consequence of crystal field. Using the spin Hamiltonian $\mathcal{H} = g\mu_B BS$, with $S = 1$, and an isotropic g-factor, an isotropic line is obtained

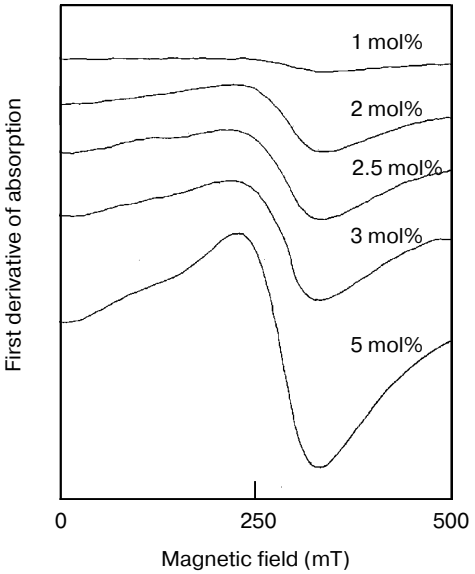

Fig. 8. EPR spectra of various mol% of Ni^{2+} ions in porous $CaSiO_3$ ceramic sample.

which corresponds to the $|M_S = 0\rangle$ and $|M_S = \pm 1\rangle$ magnetic dipole transitions. Owing to the moderately high spin–orbit coupling, the isotropic g-factor of octahedrally coordinated Ni^{2+} deviates from the free-electron value ($g_e = 2.0023$) in the framework of the ligand field theory, it is given by the relation [23, 46]:

$$g = g_e - \frac{8\lambda}{\Delta},$$

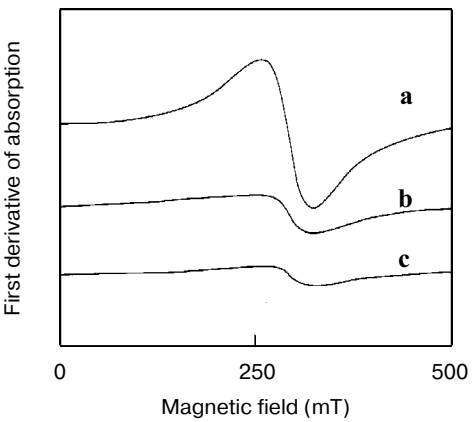

Fig. 9. EPR spectra of 1 mol% of Ni^{2+} ions in lithium-doped $CaSiO_3$ (**a**), sodium-doped $CaSiO_3$ (**b**), potassium-doped $CaSiO_3$ ceramic sample (**c**).

Table 3. Number (N) of spins participating in resonance and susceptibility (χ) as a function of Ni^{2+} content in $CaSiO_3$ ceramic powders.

Ni^{2+} (mol%)	N (10^{23}/kg)	χ (10^{-2} m^3/kg)
1.0	1.45	4.40
2.0	7.73	23.43
2.5	10.60	32.12
3.0	13.56	41.10
5.0	25.75	78.04

where λ is the effective spin–orbit coupling constant and Δ is the energy difference between the ground state $^3A_{2g}(F)$ and the excited state $^3T_{2g}(F)$. Normally the Δ value lies at about 8970 cm^{-1} [47–49]. The observed g value (2.23) can be used to evaluate the λ value and the evaluated λ value is 255 cm^{-1}, which is 76% of the free-ion value. A comparison with the free-ion value, $\lambda = -335$ cm^{-1}, suggests a certain amount of covalency. Owen's ionic parameter, α^2 can be evaluated by

$$g = 2.0023 - \frac{\alpha^2 8\lambda}{\Delta}.$$

The calculated value of $\alpha^2 = 0.761$ indicates that the bonding between the Ni^{2+} ions and the ligands is moderately covalent.

The number of spins participating in resonance and their paramagnetic susceptibilities have been evaluated as a function of nickel as well as alkali content and are presented in Tables 3 and 4, respectively. It is observed that the number of spins participating in resonance increases with nickel content whereas it decreases when size of the alkali increases.

4 Conclusions

Thermally stable macroporous $CaSiO_3$ ceramics have been prepared by the solution-combustion method. The effect of temperature on crystalline phase formation, amount of porogens and particle size of porous $CaSiO_3$ has been investi-

Table 4. Number (N) of Ni^{2+} ions participating in resonance and susceptibility (χ) as a function of alkali content in $CaSiO_3$ ceramic powders.

Alkali	N (10^{23}/kg)	χ (10^{-2} m^3/kg)
Li	8.0	24.21
Na	2.32	7.03
K	0.91	2.76

gated. Completely crystalline single-phase β-$CaSiO_3$ and α-$CaSiO_3$ ceramics have been obtained at 950 and 1200 °C, respectively. The microstructure and morphology were studied by SEM and it is interesting to note that with increase of temperature the samples become more and more porous and the pore diameter increases from 0.2 to 8 μm. The calculated porosity values are 17.5% and 31.6% at 950 and 1200 °C, respectively. The surface area of as-formed $CaSiO_3$ and calcined at 950 and 1200 °C are 31.93, 0.585 and 3.48 m^2/g, respectively. The EPR spectrum of Fe^{3+} ions in $CaSiO_3$ ceramics exhibits a weak resonance signal at $g = 4.20 \pm 0.1$, and an intense signal at $g = 2.0 \pm 0.1$. The signal at $g = 4.20$ is ascribed to isolated Fe^{3+} ions at orthorhombic site. The resonance signal at $g = 2.0$ is due to two or more Fe^{3+} ions coupled together with dipolar interaction. The EPR spectrum of Ni^{2+} ions in $CaSiO_3$ ceramics exhibits a symmetric absorption at $g = 2.23 \pm 0.01$. The site symmetry around the Ni^{2+} ions is predominantly octahedral and the bonding between the Ni^{2+} ions and the ligands is moderately covalent. The N and χ increase with iron as well as nickel content and there is no cluster formation up to 5 mol%. Further it is observed that as the size of the alkali increases, N and χ decrease.

Acknowledgments

We are thankful to the referees for their valuable critical comments and suggestions which enabled us to improve the quality of the paper. R.P.S.C. thanks H. S. Maiti, Director of Central Glass and Ceramic Research Institute (CGCRI) and K. K. Phani, head of Glass Technology Laboratory of CGCRI, for their constant encouragement.

References

1. Kresge, C.T., Leonowicz, M.E., Roth, W.J., Vartuli, J.C., Beck, J.S.: Nature **359**, 710 (1992)
2. Yang, P., Zhao, D., Margolese, D.I., Bates, B.F., Stucky, G.D.: Nature **396**, 152 (1998)
3. Zhao, D., Feng, F., Quo, Q., Melosh, N., Fredrickson, G.H., Chmelka, B.F., Stucky, G.D.: Science **279**, 548 (1999)
4. Corbin, S.F., Apte, P.S.: J. Am. Ceram. Soc. **82**, 693–701 (1999)
5. Chandrappa, G.T., Steunou, N., Livage J.: Nature, **416**, 702 (2002)
6. Shevchenko, Ya.V.: Introduction to Engineering Ceramics. Nauka, Moscow (1993)
7. Shevchenko, Ya.V., Barinov, S.M.: Engineering Ceramics. Nauka, Moscow (1993)
8. Boccaccini, A.R., Petitmermel, M., Wintermantel, E.: J. Am. Ceram. Soc. **76**, 75 (1997)
9. Kingsley, J.J., Patil, K.C.: Mater. Lett. **6**, 427 (1988)
10. Ainsworth, C., Jones, R.: J. Am. Chem. Soc. **77**, 621 (1995)
11. Chandrappa, G.T., Chandran, R.G., Patil, K.C.: Int. J. Self-Propag. High Temp. Synthes. **4**, 183 (1995)
12. Yun, Y.H., Yun, S.D., Park, H.R., Lee, Y.K., Youn, Y.N.: J. Mater. Synth. Process. **10**, 205 (2002)
13. Lin, K., Chang, J., Zeng, Y., Qian, W.: Mater. Lett. **58**, 2109 (2004)
14. Yoshizawa, J., Matushita, H., Iwamoto, K., Katsui, A.: J. Adv. Sci. **13**, 52 (2001)
15. Kanzaki, M., Stebbins, J.F., Xue, X.: Geophys. Res. Lett. **18**, 463 (1991)
16. Klug, H., Alexander L.: X-Ray Diffraction Procedures, p. 491. Wiley, New York (1962)
17. Fan, X., Wang, M., Hong, X., Qian, G.: J. Phys.: Condens. Matter **9**, 3479 (1997)
18. Ming, T.J., Lin, R.Y., Ko, Y.H.: Am. Ceram. Soc. Bull. **70**, 1167 (1991)
19. Brumauer, S., Emmete, P.H., Teller, E.: J. Am. Chem. Soc. **66**, 309 (1938)

20. Abragam, A., Bleaney, B.: Electron Paramagnetic Resonance of Transition Ions. Clarendon, Oxford (1970)
21. Pilbrow, J.R.: Transition Ion Electron Paramagnetic Resonance. Clarendon, Oxford (1990)
22. Mabbs, F.E., Collison, D.: Electron Paramagnetic Resonance of d Transition-Metal Compounds. Elsevier, Amsterdam (1992)
23. Weil, J.A., Bolton, J.R., Wertz, J.E.: Electron Paramagnetic Resonance: Elementary Theory and Practical Applications. Wiley, New York (1994)
24. Poole, C.P. Jr., Farach, H.A. (eds.): Handbook of Electron Spin Resonance. American Institute of Physics, New York (1994)
25. Poole, C.P. Jr., Farach, H.A. (eds.): Handbook of Electron Spin Resonance, vol. 2. AIP Press, New York (1999)
26. Stevens, K.W.H.: Magnetic Ions in Crystals. Princeton University Press, Princeton (1997)
27. Rudowicz, C.: Magn. Reson. Rev. **13**, 1 (1987)
28. Rudowicz, C.: Magn. Reson. Rev. **13**, 335 (1988)
29. Rudowicz, C.: J. Phys.: Condens. Matter **12**, L417 (2000)
30. Rudowicz, C., Misra S.K.: Appl. Spectrosc. Rev. **36**, 11 (2001)
31. Bleaney, B., Stevens, K.W.H.: Rep. Prog. Phys. **16**, 108 (1953)
32. Gibson, J.F., in: Norman, R.O.C. (ed.) Electron Spin Resonance, vol. 3, pp. 90–133. Specialist Periodical Reports. Chemical Society, London (1976)
33. Rudowicz, C., Bramely, R.: J. Chem. Phys. **83,** 5192 (1985)
34. Rudowicz, C.: J. Chem. Phys. **84**, 5045 (1986)
35. Rudowicz, C.: Mol. Phys. **74**, 1159 (1991)
36. Gaite, J.M., Michoulier, J.: Crystallographie **93**, 341 (1970)
37. Castner, T., Newell, G.S. Jr., Holton, W.C., Slichter, C.P.: J. Chem. Phys. **32**, 668 (1960)
38. Burzo, E., Chipara, M., Ungur, D., Ardelean, I.: Phys. Status Solidi **124**, K117 (1984)
39. Kishore, N., Bansal, T.K., Kamal, R., Mendiratta, R.G.: Phys. Chem. Glasses **25**, 52 (1984)
40. Yang, H., Prewitt, C.T.: Am. Mineral. **84**, 929 (1999)
41. Yeom, T.H., Rudowicz, C., Choh, S.H., McGavin, D.G.: Phys. Status Solidi B **198**, 839 (1996)
42. Pilbrow, J.R., Lowrey, M.R.: Rep. Prog. Phys. **43**, 434 (1980)
43. Rudowicz, C., Qin, J.: J. Lumin. **110**, 39 (2004)
44. Rao, B.G., Rao, K.J.: Chem. Phys. **102**, 121 (1986)
45. Ashcroft, N.W., Mermin, N.D.: Solid State Physics, p. 656. Harcourt Brace College Publishers, New York (1976)
46. Sreedhar, B., Sumalatha, C., Kojima, K.: J. Mater. Sci. **31**, 1445 (1996)
47. Lever, A.B.P.: Inorganic Electronic Spectroscopy. Elsevier, Ansterdam (1968)
48. Figgis, B.N.: Introduction to Ligand Fields. Wiley Eastern, New Delhi (1976)
49. Wong, J., Angell, C.A.: Glass Structure by Spectroscopy. Marcel Dekker, New York (1976)

Authors' address: R. P. Sreekanth Chakradhar, Glass Technology Laboratory, Central Glass and Ceramic Research Institute, Kolkata 700032, India
E-mail: chakra@cgcri.res.in